THEORY

Analysis and Design of High-Frequency WPT System Using Load-Independent Inverter With Robustness Against Load Variations and Coil Misalignment

YUTARO KOMIYAMA [1], (Graduate Student Member, IEEE), AYANO KOMANAKA[1],
HIROAKI OTA[2], YUKI ITO [2], TAICHI MISHIMA [2], TAKESHI UEMATSU [2],
AKIHIRO KONISHI[1], (Member, IEEE), WENQI ZHU [1], (Member, IEEE),
KIEN NGUYEN [1], (Senior Member, IEEE), AND
HIROO SEKIYA [1], (Senior Member, IEEE)

[1]Graduate School of Science and Engineering, Chiba University, Chiba 263-8522, Japan
[2]Omron Corporation, Kyoto 619-0238, Japan

Corresponding author: Hiroo Sekiya (sekiya@faculty.chiba-u.jp)

ABSTRACT This paper presents an analysis and design of the load-independent (LI) high-frequency magnetic resonant wireless power transfer (MR-WPT) system with robustness against load variations and coil misalignments. It is clarified from the analysis that robustness against load variations and coil misalignment can be obtained when LI inverter, series-resonant to series-resonant (S-S) coupling topology, input-reactance invariant rectifier against load variations, and post regulator are adopted. The output reactance of the transmitter does not vary against load variations and coil misalignment. Therefore, the inverter works with the LI mode, achieving soft switching without control. As a result, the system ensures soft switching and output regulation against both load variations and coil misalignment without wireless communication feedback. The design example of the system with LI class-E/F inverter, class-D rectifier, and buck converter is given. The quantitative agreements between the analytical prediction and experiment show the effectiveness and validity of the system and its analysis.

INDEX TERMS Class-E/F inverter, coil misalignment, load-independent, post regulator, wireless power transfer.

I. INTRODUCTION

Advancing the social implementation of magnetic resonant wireless power transfer (MR-WPT) systems is the critical topic in realizing a wireless society. Research for making WPT technology practical has been conducted in various applications, including drones [1], implantable medical devices [2], and wearable devices [3]. These applications demand downsizing and lightweighting of the circuits.

The associate editor coordinating the review of this manuscript and approving it for publication was Harikrishnan Ramiah .

A high-frequency operation is effective for miniaturizing the circuit because it can reduce the passive components' size. Meanwhile, high-frequency operation raises challenges, such as a requirement for fast feedback control and large switching losses. Because the switching losses are proportional to the transmission frequency [4], there is a trade-off between system miniaturization due to the increase in transmission frequency and efficiency degradation due to the switching losses. For realizing high-frequency and high-efficiency operation simultaneously, the soft switching technique, namely zero-voltage switching (ZVS) or zero-current switching

(ZCS), is essential, which can suppress switching loss. Under the soft switching operation, the efficiency degradation can be reduced, and we can obtain the benefit of the system miniaturization at high frequencies.

In high-frequency WPT systems, power management [5], [6], [7], [8] is one of the most significant research challenges recently. The output regulation and the soft switching against load variations and coil misalignment must be maintained. In [9] and [10], a maximum efficiency tracking control has been proposed for the WPT with the class-E inverter. The systems achieve soft switching over a wide range of load variations and coil misalignments by adopting a pre- or post-regulator. However, they require information feedback from the receiver to the transmitter. The feedback signal should be transmitted by wireless communications in the MR-WPT systems. The communication delays degrade the transient response performance of the control against sudden load changes and coil misalignments. In addition, the communication delays include unpredictable jitter. Therefore, the system cannot guarantee high reliability using feedback communication [11].

There has been extensive research on load-independent (LI) operation [12], [13], [14], [15], [16], [17], [18], which can eliminate the need for wireless communication from the WPT systems. The concept of the 'load-independent' was proposed for class-E inverter in 1990 [12]. At that time, the class-E inverters were intended for applications such as amplifiers for communication equipment and inverter parts of DC/DC converters. The communication equipment operates at fixed load resistance [19]. Besides, the DC/DC converters commonly used frequency-modulated controls to achieve soft switching and output regulation [20]. Hence, the LI operation did not attract much attention. Since the breakthrough on the MR-WPT system in 2007 [21], research on WPT systems has rapidly increased. The WPT systems raised the demand for responding to load variations without feedback communication and complex control. Besides, the fixed frequency operation is also desired for Industrial Scientific and Medical (ISM) frequency band operation. Therefore, the LI class-E inverter, which achieves soft switching and constant AC output regardless of the load resistance, has attracted attention. Now, the LI operation has also been applied to several high-frequency inverters, such as class-Φ [13], class-E/F [14], and class-E^{-1} [15] inverters.

The WPT systems with LI high-frequency inverters achieve soft switching and constant voltage (CV) or constant current (CC) output against load variations [22], [23]. For applying the LI high-frequency inverters [12], [13], [14], [15], [16], [17], [18] to the WPT system, a general design guideline has been presented [24]. The criteria for selecting an inverter and a rectifier is shown according to the coupling type of the resonant circuit, namely series-resonant to series-resonant (S-S), series-resonant to parallel-resonant (S-P), P-S, and P-P couplings. The LI high-frequency WPT system in [24], however, does not support the soft switching and output regulation against coil misalignment. The output voltage varies

depending on the coupling coefficient between the transmitter and receiver coils. In addition, the coupling-coefficient variations generally cause variations in the output reactance of the inverter. Therefore, soft switching is not guaranteed against coil misalignments. It is essential to establish a design guideline for the LI high-frequency WPT system, which is robust against load variations and coil misalignments.

This paper presents an analysis and design of the LI high-frequency MR-WPT system with robustness against load variations and coil misalignments. The proposed system achieves soft switching and consistent output-voltage regulation against both load variations and coil misalignment without feedback communication. This paper analyzes a WPT system consisting of the LI high-frequency inverter, coupling part, rectifier, and post regulator. The analysis reveals that robustness can be acquired when adopting the S-S coupling topology and input-reactance invariant rectifier against load variations. The inverter works with the LI mode even against coil misalignment because the output reactance of the transmitter is consistent in the proposed configuration. This paper shows a concrete design example of the MR-WPT system with LI class-E/F inverter, class-D rectifier, and buck converter, along with its analytical expressions. The experimental prototype achieved soft switching and output-voltage regulation against load variations and coil misalignment. The experimental results were in quantitative agreement with the analytical predictions, which showed the validity of the analysis and design.

II. LI HIGH-FREQUENCY INVERTER
The LI high-frequency inverters achieve soft switching and constant AC output regardless of the load resistance. Table 1 gives the LI high-frequency inverters and their characteristics. Depending on the topology, they exhibit different features in switching types, output, and resonant filters. The diversity of topologies and characteristics offers a wide range of applications. For example, the ZVS is useful in high-frequency applications where the parasitic capacitance of the switching device must be considered [25]. On the other hand, the ZCS is effective in suppressing current-related turn-off losses [15]. Additionally, the CC output with a series resonant filter and CV output with a parallel resonant filter are preferred in WPT applications [22] in terms of overcurrent protection of the transmitter coil against coil misalignment.

TABLE 1. LI high-frequency inverters.

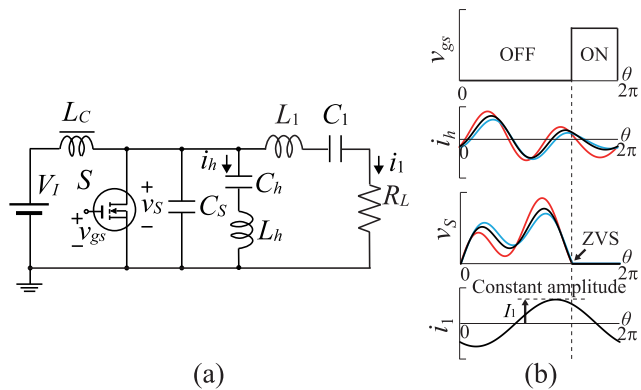|	Switching type	Output	Resonant filter
Class-E [12]	ZVS	CV	Series
Class-Φ [13]	ZVS	CV	Series
Class-E/F [14]	ZVS	CC	Series
Class-E^{-1} [15]	ZCS	CV	Parallel
Class-E [16]	ZVS	CC	Parallel
Class-E^{-1} [17]	ZCS	CC	Series
Class-E [18]	ZVS	CC	Parallel

FIGURE 1. The LI class-E/F inverter. (a) Circuit topology. (b) Example waveforms for fixed load resistance (black line: $R_L/R_{Lr} = 1$, blue line: $R_L/R_{Lr} = 0.5$, red line: $R_L/R_{Lr} = 2$).

A. LI OPERATION

As an example of the LI high-frequency inverter, we illustrate the LI class-E/F inverter [14]. Fig. 1 shows the circuit topology and example waveforms of the LI class-E/F inverter, where θ is the angular time, and the subscript 'r' of R_{Lr} means its rated value. The LI class-E/F inverter achieves soft switching and constant amplitude of output current regardless of the load resistance, as shown in Fig. 1(b). The LI operation is obtained by using the appropriate component values. The component values can be determined analytically [14], which satisfy the conditions as

$$v_S(2\pi D_S) = 0, \tag{1}$$

and

$$\frac{dI_1}{dR_L} = 0, \tag{2}$$

where Ds is the off-duty ratio of the switch, I_1 is the amplitude of the output current, and R_L is the load resistance of the inverter.

B. APPLICATION FOR WPT SYSTEMS

The LI high-frequency inverters are applied to a transmitter of the WPT systems [22], [23], [24]. The LI high-frequency WPT systems achieve soft switching and constant output against load variations without feedback communication. Although there are WPT systems that achieve constant output without controls using class-D inverter [26], [27], they cannot achieve soft switching against load variations. Therefore, the LI inverters given in Table 1 are more suitable for high-frequency WPT systems. However, the LI high-frequency WPT systems cannot achieve constant output against coil misalignment. This paper investigates the appropriate configuration of the WPT system with the LI high-frequency inverter that simultaneously accommodates load variations and coil misalignments.

III. LI WPT SYSTEM WITH POST REGULATOR

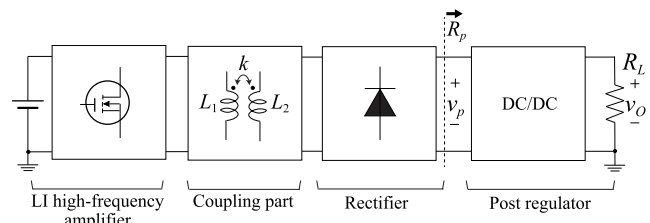Fig. 2 shows a configuration of the LI high-frequency WPT system with the post regulator, which consists of LI

FIGURE 2. Circuit configuration of the LI high-frequency WPT system with post regulator.

high-frequency inverter, coupling part, rectifier, and post regulator. The proposed WPT system is designed to achieve soft switching and output regulation against load variations and coil misalignment.

A. INVERTER

It is a prerequisite that the LI high-frequency inverter listed in Table 1 is adopted for the transmitter in this paper. This is because we would like to use the automatic soft-switching characteristic against load variations. The LI high-frequency inverter achieves soft switching against variations in load resistance. Meanwhile, it cannot maintain soft switching against variations in reactance components of output resonant filter [28]. Therefore, we investigate how the load variations, coil misalignments, and output regulation affect the equivalent inductance seen from the inverter in the proposed WPT configuration.

B. POST REGULATOR

The post regulator has a role in regulating the output voltage to the rated value. The input resistance of the post regulator can be expressed as

$$R_p = \frac{V_p^2 R_L}{V_O^2} = \frac{R_L}{M_p^2}, \tag{3}$$

where V_p and V_O are the input and output voltages of the post regulator, R_L is the load resistance, and M_p is the voltage gain of the post regulator. The output regulation is conducted by changing the voltage gain M_p. Besides, the load variations are attributed to the variations in R_L. From (3), the load variations and output regulation can be regarded as the variations in the input resistance of post-regulator R_p.

C. RECTIFIER

There are basically two types of rectifiers in the high-frequency WPT system, which are current-driven rectifiers with series resonance, as shown in Fig. 3(a) and (c), and voltage-driven rectifiers with parallel resonance, as shown in Fig. 3(b) and (d) [29]. The rectifiers have an input impedance whose resistive component is proportional to the output resistance. From (3), the input impedance of the current-driven rectifier can be modeled as [29]

$$\dot{Z}_{rct} = R_{rct} + \frac{1}{j\omega C_{rct}} = \frac{\alpha_{cd} R_L}{M_p^2} + \frac{1}{j\omega C_{rct}}, \tag{4}$$

TABLE 2. The analytical expressions of the equivalent impedance seen from the inverter and resonant condition for achieving LI operation.

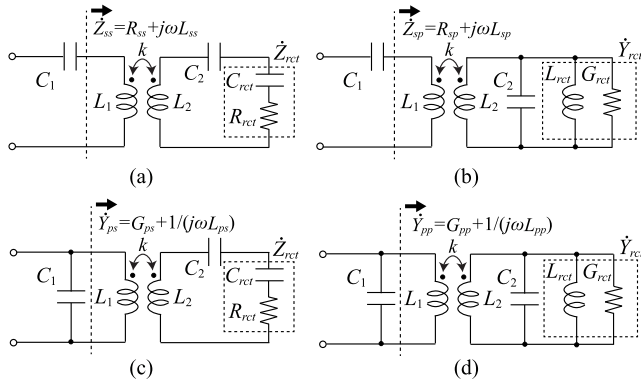| Coupling type	Resistive component	Reactance component	Resonant condition	Output voltage
S-S	$R_{ss} = \frac{k^2\omega^2 L_1 L_2}{\alpha_{cd}R_L}$	$L_{ss} = L_1$	$\omega = \frac{1}{\sqrt{L_2(C_2+C_{rct})}}$	$V_O = \omega k I_1\sqrt{\frac{L_1 L_2}{2\alpha_{cd}}}$
S-P	$R_{sp} = \frac{k^2 L_1 \alpha_{vd} R_L}{L_2}$	$L_{sp} = (1-k^2)L_1$	$\omega = \frac{1}{\sqrt{(L_2+L_{rct})C_2}}$	$V_O = \frac{V_1}{k}\sqrt{\frac{L_2}{2L_1\alpha_{vd}}}$
P-S	$G_{ps} = \frac{k^2 L_2}{L_1\alpha_{cd}R_L}$	$L_{ps} = L_1$	$\omega = \frac{1}{\sqrt{(1-k^2)L_2(C_2+C_{rct})}}$	$V_O = kV_1\sqrt{\frac{L_2}{2L_1\alpha_{cd}}}$
P-P	$G_{pp} = \frac{k^2\alpha_{vd}R_L}{\omega^2(1-k^2)^2 L_1 L_2}$	$L_{pp} = (1-k^2)L_1$	$\omega = \sqrt{\frac{1}{(1-k^2)L_2 C_2}+\frac{1}{L_{rct}C_2}}$	$V_O = \frac{\omega(1-k^2)I_1}{k}\sqrt{\frac{L_1 L_2}{2\alpha_{vd}}}$

FIGURE 3. Coupling types of the WPT system. (a) S-S. (b) S-P. (c) P-S. (d) P-P.

where ω is the angular transmission frequency and α_{cd} is a constant. Besides, in voltage-driven topology, the input admittance of the rectifier can be modeled using (3) as [29]

$$\dot{Y}_{rct} = G_{rct} + \frac{1}{j\omega L_{rct}} = \frac{\alpha_{vd}M_p^2}{R_L} + \frac{1}{j\omega L_{rct}}, \qquad (5)$$

where α_{vd} is a constant.

There are particular rectifiers whose input reactance or input susceptance is independent of the load resistance. For example, class-D [29] and LI class-E, and LI class-E/F rectifiers[1] have this characteristic. The class-D rectifier works with diodes. On the other hand, the LI class-E and LI class-E/F rectifiers need synchronous rectifications.

D. COUPLING PART
Fig. 3 shows the basic coupling types of the WPT system. They are classified by the resonant structure: S-S, S-P, P-S, and P-P. In [24], the condition for achieving the LI operation of the inverter is presented for each coupling type solely against load variations, which is given in Table 2. However, there is no discussion concerning the coil misalignment. In addition, the coupling-coefficient variations generally cause simultaneous variations in the output impedance of the

[1]The class-E and E/F inverters have an inductive output resonant filter. In the LI class-E and E/F inverters, the output reactance, that is, an extra inductive component, is independent of the load resistance [22]. Meanwhile, there is a time-reverse duality between the inverter and rectifier waveforms [24]. Therefore, it can be stated that the input reactance of the LI class-E and E/F rectifiers is independent of the load resistance.

inverter. Meanwhile, the LI operation of the class-E inverter family only supports resistive component variations. This paper discusses the feasibility of designing a robust WPT system for both load variations and coil misalignment with the configuration in Fig. 2.

1) S-S COUPLING
The equivalent impedance seen from the transmitter in S-S coupling is given in (6), as shown at the bottom of the next page. The load variations and the impedance transformation of the post regulator are both reflected in the variations of R_{rct} and C_{rct}. Besides, the coil misalignment is expressed as the variation of coupling coefficient k.

For keeping the LI operation against the load variations and coil misalignment, the equivalent inductance L_{ss} must be constant [24]. Therefore, it is necessary to consider resonant conditions such that L_{ss} becomes constant, independent of R_{rct}, C_{rct}, and k.

When the rectifier series-resonant filter satisfies

$$\frac{1}{\sqrt{L_2(C_2+C_{rct})}} - \omega = 0, \qquad (10)$$

the equivalent resistance and inductance are

$$R_{ss} = \frac{\omega^2 k^2 L_1 L_2 M_p^2}{\alpha_{cd}R_L}, \qquad (11)$$

and

$$L_{ss} = L_1, \qquad (12)$$

respectively. From (10) and (12), the equivalent inductance is constant when C_{rct} is independent of R_p. In this case, the variations in R_L and k can be reflected only on R_{ss}. Additionally, the post-regulator determines M_p to keep the output voltage constant.

As discussed, the S-S coupling WPT system is robust against load variations and coil misalignment when the rectifier has an input series-resonant filter satisfying the condition in (10) and an input-reactance invariant against load resistance.

2) S-P COUPLING
The equivalent impedance seen from the transmitter in S-P coupling is expressed in (7), as shown at the bottom of the next page.

For example, when the input parallel-resonant filter of the rectifier safeties

$$\frac{1}{\sqrt{C_2(L_2 + L_{rct})}} - \omega = 0, \qquad (13)$$

the equivalent inductance is expressed as

$$L_{sp} = (1 - k^2)L_1. \qquad (14)$$

We see from (14) that the inverter cannot maintain LI operation because L_{sp} depends on k.

Also, when the condition

$$\left(\frac{1}{\omega L_{rct}} - \omega C_2\right)\left[\frac{1}{\omega(L_2 + L_{rct})} - \omega C_2\right] + G_{rct}^2 = 0, \quad (15)$$

is satisfied, the equivalent inductance becomes

$$L_{sp} = L_1. \qquad (16)$$

Although there is no coupling coefficient k in (16), the equivalent conductance G_{rct} is included in (15). The G_{rct} is a function of R_L and M_p and varies to keep the output voltage constant against load variations and coil misalignment. Therefore, the resonant condition (15) cannot be satisfied for load variations and coil misalignment. As a result, it is impossible to keep the equivalent inductance constant against load variation and coil misalignment in S-P coupling.

Similarly, we can see from the equivalent admittance expressions for P-S and P-P couplings in (8) and (9), as shown at the bottom of the page, that the equivalent susceptances must depend on load resistance and coupling coefficient. Therefore, the WPT system in Fig. 2 can maintain soft switching and output regulation against load variations and coil misalignment only for the S-S coupling topology.

E. OUTPUT VOLTAGE FOR S-S COUPLING
By considering the power relationship, we have

$$\frac{R_{ss}I_1^2}{2} = \frac{V_O^2}{R_L}, \qquad (17)$$

where I_1 is the amplitude of AC flowing through the transmitter coil L_1. From (11) and (17), the output voltage V_O can be expressed as

$$V_O = \omega k M_p I_1 \sqrt{\frac{L_1 L_2}{2\alpha_{cd}}}. \qquad (18)$$

We see from (18) that the output voltage is regulated only by adjusting M_p against variations of R_L, k, and I_1. By comparing the expression of the output voltage for S-S coupling in Table 2 and (18), we can confirm that the proposed WPT system has the capability of achieving the output-voltage regulation for both load variations and coil misalignment, though it cannot be achieved in the WPT system in [24].

Because of the automatic soft switching achievement, the WPT achieves output regulation and high power-delivery efficiency against load variations and coil misalignment without wireless communication feedback, which can be explained theoretically.

IV. LI CLASS-E/F WPT SYSTEM WITH BUCK CONVERTER
Fig. 4 shows the WPT system designed in this paper, which consists of the LI class-E/F inverter, S-S coupling part, current-driven class-D rectifier, and buck converter. The system guarantees ZVS at the inverter and output-voltage regulation against load variations and coil misalignment without feedback from the receiver to the transmitter.

Fig. 5 shows typical waveforms of the system. The class-E/F inverter has a harmonic resonant filter L_h-C_h connected to the switch in parallel. It generates the harmonic current as shown in Fig. 5(a), suppressing the switch-voltage stress [30]. The waveforms in the transmitter do not change with coil misalignment due to the impedance transformation. Besides, the inverter works with LI mode under the output regulation. Therefore, the class-E/F inverter always satisfies the

$$\dot{Z}_{ss} = R_{ss} + j\omega L_{ss} = \frac{\omega^2 k^2 L_1 L_2 \alpha_{cd} M_p^2 R_L}{\alpha_{cd}^2 R_L^2 + M_p^4\left[\omega L_2 - \frac{1}{\omega(C_2+C_{rct})}\right]^2} + j\omega L_1\left\{1 - \frac{\omega k^2 L_2 M_p^4\left[\omega L_2 - \frac{1}{\omega(C_2+C_{rct})}\right]}{\alpha_{cd}^2 R_L^2 + M_p^4\left[\omega L_2 - \frac{1}{\omega(C_2+C_{rct})}\right]^2}\right\} \qquad (6)$$

$$\dot{Z}_{sp} = R_{sp} + j\omega L_{sp} = \frac{k^2 L_1 \alpha_{vd} M_p^2 R_L}{L_2\left\{\alpha_{vd}^2 M_p^4 + R_L^2\left[\frac{1}{\omega(L_2+L_{rct})} - \omega C_2\right]^2\right\}} + j\omega L_1\left\{1 - k^2 - \frac{\frac{k^2 R_L^2 L_2}{\omega L_{rct}(L_2+L_{rct})}\left[\frac{1}{\omega(L_2+L_{rct})} - \omega C_2\right]}{\alpha_{vd}^2 M_p^4 + R_L^2\left[\frac{1}{\omega(L_2+L_{rct})} - \omega C_2\right]^2}\right\} \qquad (7)$$

$$\dot{Y}_{ps} = G_{ps} + \frac{1}{j\omega L_{ps}} = \frac{\omega k^2 L_2 \alpha_{cd} M_p^2 R_L - j\left\{\alpha_{cd}^2 R_L^2 + M_p^4\left[\omega L_2 - \frac{1}{\omega(C_2+C_{rct})}\right]\left[\omega(1-k^2)L_2 - \frac{1}{\omega(C_2+C_{rct})}\right]\right\}}{\omega L_1\left\{\alpha_{cd}^2 R_L^2 + M_p^4\left[\omega(1-k^2)L_2 - \frac{1}{\omega(C_2+C_{rct})}\right]^2\right\}} \qquad (8)$$

$$\dot{Y}_{pp} = G_{pp} + \frac{1}{j\omega L_{pp}} = \frac{k^2 \alpha_{vd} M_p^2 R_L + j\omega L_2\left\{R_L^2\left[\omega C_2 - \frac{1}{\omega(L_2+L_{rct})}\right]\left[\frac{1}{\omega L_2} - (1-k^2)\left(\omega C_2 - \frac{1}{\omega L_{rct}}\right)\right] - (1-k^2)\alpha_{vd}^2 M_p^4\right\}}{\omega^2 L_1 L_2\left\{(1-k^2)^2 \alpha_{vd}^2 M_p^4 + R_L^2\left[\frac{1}{\omega L_2} - (1-k^2)\left(\omega C_2 - \frac{1}{\omega L_{rct}}\right)\right]^2\right\}} \qquad (9)$$
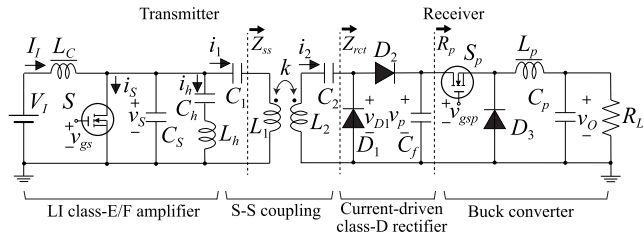
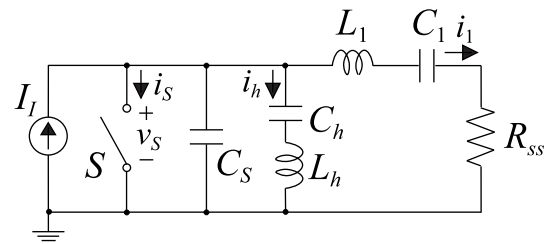**FIGURE 4.** Circuit topology of the design example of the proposed WPT system.
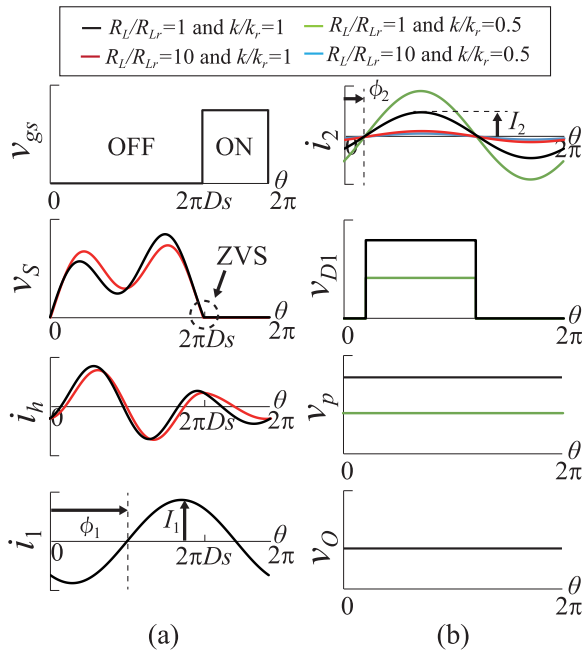

FIGURE 5. Superimposed waveforms of the design example of the proposed system for fixed load resistance and coupling coefficient. (a) Transmitter side. (b) Receiver side.

ZVS condition at the turn-on instant and constant amplitude of the transmission current.

The current-driven class-D rectifier has two diodes, whose voltages are the square wave as shown in Fig. 5(b). The rectifier output voltage becomes a DC voltage through the filter capacitance C_f, independent of the load resistance but depends on the coupling coefficient k. Therefore, the output voltage is regulated by the PWM-controlled buck converter against coil misalignment, whose on-duty ratio is Ds_p.

A. BUCK CONVERTER
This paper adopts the traditional buck converter [31]. The input resistance of the buck converter is

$$R_p = \frac{R_L}{M_p^2} = \frac{R_L}{Ds_p^2}. \quad (19)$$

B. CURRENT-DRIVEN CLASS-D RECTIFIER
When the input current of the rectifier can be assumed as a pure sinusoid, namely

$$i_2(\theta) = I_2 \sin(\theta + \phi_2), \quad (20)$$

FIGURE 6. Analytical model of the LI class-E/F inverter.

where I_2 is the amplitude of current i_2 and ϕ_2 is the phase shift from the gate-drive voltage, as shown in Fig 5(b). The output voltage of the rectifier is

$$V_p = \frac{R_p}{2\pi} \int_{-\phi_2}^{\pi-\phi_2} I_2 \sin(\theta + \phi_2) d\theta = \frac{R_p I_2}{\pi} = \frac{R_L I_2}{\pi Ds_p^2}. \quad (21)$$

From (21), the input resistance of the class-D rectifier [29] is obtained as

$$R_{rct} = \frac{2R_p}{\pi^2} = \frac{2R_L}{\pi^2 Ds_p^2}. \quad (22)$$

Note that the input impedance of the current-driven class-D rectifier has no reactance component.

From (11) and (22), the input resistance seen from the transmitter can be expressed as

$$R_{ss} = \frac{\pi^2 Ds_p^2 \omega^2 k^2 L_1 L_2}{2R_L}. \quad (23)$$

C. LI CLASS-E/F INVERTER
Fig. 6 shows the analytical model of the LI class-E/F inverter. In this analysis, the analytical procedure and assumptions are based on [16]. The output current of the class-E/F inverter is assumed as

$$i_1(\theta) = I_1 \sin(\theta + \phi_1), \quad (24)$$

where ϕ_1 is the phase shift from the gate-drive voltage.

By solving piece-wise linear differential equations, we can obtain the waveform equations of the current flowing through L_h as

$$i_h(\theta) = \begin{cases} A_1 \cos(\sqrt{\gamma+1}\omega_h\theta) + B_1 \sin(\sqrt{\gamma+1}\omega_h\theta) \\ +\dfrac{\gamma\omega_h^2 I_1 \sin(\theta+\phi_1)}{1-(\gamma+1)\omega_h^2} + \dfrac{\gamma I_I}{\gamma+1} \text{ for } 0 \le \theta < 2\pi D_S, \\ A_2 \cos(\omega_h\theta) + B_2 \sin(\omega_h\theta) \text{ for } 2\pi D_S \le \theta < 2\pi, \end{cases}$$
$$(25)$$

respectively, where A_1, B_1, A_2, and B_2 are the unknown constants, which can be obtained analytically from the boundary conditions of i_h and its derivative, $\gamma = C_2/C_S$ is the ratio of capacitances, $\omega_h = 1/(\omega\sqrt{L_h C_h})$ is the normalized harmonic resonant frequency, and I_I is the input current.

From KCL and (25), the switch current is obtained as

$$
i_S(\theta) = \begin{cases} 0 \text{ for } 0 \leq \theta < 2\pi D_S, \\ -A_2 \cos(\omega_h\theta) - B_2 \sin(\omega_h\theta) - I_1 \sin(\theta + \phi_1) + I_I \\ \quad \text{for } 2\pi D_S \leq \theta < 2\pi, \end{cases}
$$

$$(26)$$

By integrating the current flowing through shunt capacitance C_S, we have (27), as shown at the bottom of the page.

For achieving (1) and (2), it is necessary to satisfy

$$\phi_1 = -\pi Ds, \tag{28}$$

$$\omega_h = \frac{1}{2(1 - Ds)}, \tag{29}$$

and

$$
2\gamma \sin\left(\frac{\pi Ds\sqrt{\gamma+1}}{1-Ds}\right)
$$
$$
+ \frac{\pi Ds\sqrt{\gamma+1}}{1-Ds}\left[1 + \cos\left(\frac{\pi Ds\sqrt{\gamma+1}}{1-Ds}\right)\right] = 0. \tag{30}
$$

The component values can be determined uniquely from (28)-(30) and design specifications. By substituting the obtained parameters into (24)-(27), the steady-state waveforms are given. For example, the amplitude of the output current for $Ds = 0.7$ is derived as

$$I_1 \approx 15.3 \times fC_S V_I. \tag{31}$$

D. OUTPUT VOLTAGE
From (18), (22), and (31), the WPT output voltage can be expressed as

$$V_O = \frac{\pi Ds_p I_1 \omega k\sqrt{L_1 L_2}}{2} \approx 151 \times Ds_p f^2 kC_S \sqrt{L_1 L_2} V_I. \tag{32}$$

We can see from (32) that the output voltage is independent of the load resistance, which indicates that the buck converter works with a fixed duty ratio against load variations. Besides, the output regulation for coil misalignment can be realized by keeping the product kDs_p constant. Therefore, the back converter performs the impedance transformation against coil misalignment to keep the input resistance R_{ss} constant, as shown in (23).
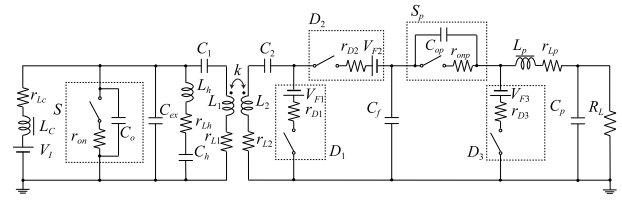

FIGURE 7. Power-loss model of the LI class-E/F WPT system with post regulator.

E. POWER DELIVERY EFFICIENCY
Fig. 7 shows the power-loss model of the LI class-E/F WPT system with the post regulator. The power delivery efficiency is estimated using the analytical waveform equations. The power loss in the equivalent series resistances (ESRs) of the inductances, diodes, and switching devices are considered, which can be calculated by following the power-loss analysis in [16].

This paper adopts the GaN HEMT for the switch S because of the ISM-band operation. Therefore, the output-capacitance hysteresis loss [32] is included in the switching-device loss as

$$P_{CO} = k_o f^{\alpha_o} V_{Smax}^{\beta_o}, \tag{33}$$

where k_o, α_o, and β_o are the coefficients of the hysteresis loss, and V_{Smax} is the maximum value of the switch voltage.

The power delivery efficiency can be predicted as

$$\eta = \frac{P_O}{P_O + P_{loss}}, \tag{34}$$

where P_{loss} is the sum of all the power-loss factors given above and P_O is the WPT output power, which is expressed as

$$P_O = \frac{V_O^2}{R_L}. \tag{35}$$

V. EXPERIMENTAL VERIFICATIONS
This section shows the experimental verifications to confirm the effectiveness of the LI high-frequency WPT system with the post regulator. The LI WPT system without a post regulator was also designed for comparison. The experiment for the two systems was conducted under the same rated condition.

The WPT system as show in Fig. 2 was implemented with the design specifications: transmission frequency $f = 6.78\ MHz$, input voltage $V_I = 80\ V$, rated load resistance $R_{Lr} = 14.7\ \Omega$, rated coupling coil distance $d_{cr} = 15\ mm$, and output voltage $V_{Or} = 16.8\ V$. The rated output voltage of the

$$
v_S(\theta) = \begin{cases} -\frac{1}{\omega C_S}\left\{\dfrac{A_1 \sin(\sqrt{\gamma+1}\omega_h\theta) + B_1[1 - \cos(\sqrt{\gamma+1}\omega_h\theta)]}{\sqrt{\gamma+1}\omega_h} - \dfrac{\theta I_I}{\gamma+1}\right. \\ \left. -\dfrac{(1-\omega_h{}^2)I_1[\cos(\theta+\phi_1) - \cos\phi_1]}{1-(\gamma+1)\omega_h{}^2}\right\} \text{ for } 0 \leq \theta < 2\pi D_S, \\ 0 \text{ for } 2\pi D_S \leq \theta < 2\pi \end{cases}
$$

$$(27)$$

system is ensured even if the load resistance and coil distance vary in the ranges of $1 \leq R_L/R_{Lr} \leq 10$ and $1 \leq d_c/d_{cr} \leq 2$, respectively. The off-duty ratio of the class-E/F inverter Ds is 0.7 [22]. Additionally, the operating frequency and the lower and upper bounds of the duty ratio of the buck converter are specified as $f_p = 200\ MHz$, $Ds_{plb} = 0.1$, and $Ds_{pub} = 0.9$.

The coupling coils L_1 and L_2 are solenoid type with air cores, whose diameters and heights are given as: $d_1 = 50\ mm$, $d_2 = 46\ mm$, and $h_1 = h_2 = 15\ mm$, respectively.

A. DESIGN AND OPTIMIZATION

The optimal designs of the system were carried out in the sense of maximizing efficiency at the rated condition. A set of parameters $\boldsymbol{x} = [N_1, N_2, d_{w1}, d_{w2}, Ds_{pr}]^T$ is given as the optimized parameter, where N_1 and N_2 are winding numbers, and d_{w1} and d_{w2} are the wire diameters of the coupling coils. When the geometric coil parameters are determined with the specified coil distance and size, theoretical self-inductances [33], ESRs [34], and coupling coefficient [35] can be obtained. The L_1, L_2, k, and Ds_{pr} determine the rated output voltage as given in (32). Meanwhile, the overall efficiency strongly depends on the ESRs. Namely, $\boldsymbol{x} = [N_1, N_2, d_{w1}, d_{w2}, Ds_{pr}]^T$ affects the output voltage and the efficiency simultaneously. Therefore, these parameters are used for maximizing efficiency while achieving output-voltage regulation.

1) OVERVIEW OF PARTICLE SWARM OPTIMIZATION

For obtaining the optimal value of $\boldsymbol{x}$, the particle swarm optimization (PSO) algorithm [36] was adopted in this paper. The PSO is one of the heuristic optimizations whose algorithm is inspired by swarms searching for food. The PSO uses multiple particles for the search. Information about the best solution is shared among the particles. The behavior of the particles is determined by the information.

Fig. 8 shows the flowchart of the PSO [36]. The position $\boldsymbol{x}_i$ and velocity $\boldsymbol{v}_i$ of particles are iteratively updated according to the evaluation function. The PSO does not require explicit initial values of $\boldsymbol{x}_i$ and $\boldsymbol{v}_i$ because they are set randomly. In addition, the algorithm does not require a calculation of partial derivatives.

The position and velocity vectors of i-th particle are given as

$$\boldsymbol{x}_i = [x_{i,1}, x_{i,2}, \cdots, x_{i,m}]^T, \qquad (36)$$

and

$$\boldsymbol{v}_i = [v_{i,1}, v_{i,2}, \cdots, v_{i,m}]^T, \qquad (37)$$

where m denotes the dimensions of the search space. The i-th particle retains the best solution $\boldsymbol{\lambda}_{p,i}$ found in its search and its evaluation value $F(\boldsymbol{\lambda}_{p,i})$. Besides, the best solution $\boldsymbol{\lambda}_g$ found in the search for all particles and its evaluation value $F(\boldsymbol{\lambda}_g)$ are retained for the entire particle swarm. At the n-th iteration, the position vector of the particle is updated as

$$\boldsymbol{x}_i^{n+1} = \boldsymbol{x}_i^n + \boldsymbol{v}_i^{n+1}. \qquad (38)$$
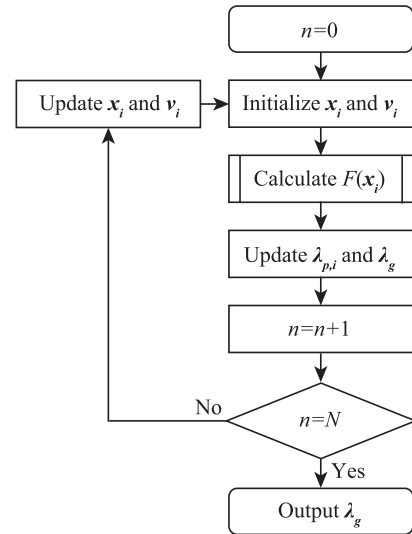
FIGURE 8. Flowchart of PSO algorithm.

The velocity vector is updated as

$$\boldsymbol{v}_i^{n+1} = w_1\boldsymbol{v}_1^n + w_2\boldsymbol{u}_2(\boldsymbol{\lambda}_{p,i}^n - \boldsymbol{x}_i^n) + w_3\boldsymbol{u}_3(\boldsymbol{\lambda}_g^n - \boldsymbol{x}_i^n), \quad (39)$$

where w_1, w_2, and w_3 are weight parameters, and $\boldsymbol{u}_2$ and $\boldsymbol{u}_3$ are m-dimensional vectors with each component uniformly distributed between 0 and 1. After N-th iterations, the optimized parameter $\boldsymbol{\lambda}_g$ can be obtained.

2) COMPONENT VALUES

From the specifications and $\boldsymbol{x}$, the component values of the system are uniquely determined for satisfying the LI conditions (28)-(30) as

$$C_S = \frac{V_{Or}}{151 \times D_{S_p}f^2k\sqrt{L_1L_2}V_I}, \qquad (40)$$

$$C_h = 0.764 \times C_S, \qquad (41)$$

$$L_h = \frac{1}{110 \times f^2C_h}, \qquad (42)$$

$$C_1 = \frac{C_S}{39.5 \times f^2L_1C_S - 0.342}, \qquad (43)$$

and

$$C_2 = \frac{1}{39.5 \times f^2L_2}. \qquad (44)$$

As a result, the power delivery efficiency can be predicted analytically as given in Section IV-E. For obtaining the optimal value of $\boldsymbol{x}$, the PSO algorithm [36], which is one of the most familiar heuristic optimizations, was adopted in this paper.

The duty ratio of the post regulator must fall within the specified range of $Ds_{plb} \leq Ds_p \leq Ds_{pub}$ even when the coil misalignment occurs. The maximum duty ratio of the regulator Ds_{pmax} appears when the coupling coefficient becomes minimum value k_{min}. Besides, the minimum duty ratio Ds_{pmin} appears at the rated coil distance.

TABLE 3. Circuit parameters derived by the optimization.

	N_1	N_2	d_{w1}	d_{w2}	Ds_{pr}
Without post regulator	5	3	0.812 mm	1.02 mm	-
With post regulator	6	6	1.22 mm	1.02 mm	0.39

TABLE 4. Analytical and experimental component values of the WPT system with and without post regulator.

	Without post regulator			With post regulator	
	Analytical	Experiment		Analytical	Experiment
L_h	1.19 μH	1.20 μH	L_h	1.19 μH	1.20 μH
L_1	1.67 μH	1.73 μH	L_1	2.41 μH	2.43 μH
L_2	0.537 μH	0.586 μH	L_2	2.15 μH	2.18 μH
C_S	191 pF	80 pF	C_S	217 pF	95 pF
C_h	146 pF	146 pF	C_h	166 pF	164 pF
C_1	744 pF	744 pF	C_1	352 pF	355 pF
C_2	940 pF	940 pF	C_2	253 pF	253 pF
C_f	-	100 ˉF	C_f	-	100 μF
r_{L_h}	-	368 mΩ	r_{L_h}	-	344 mΩ
r_{L_1}	339 mΩ	249 mΩ	r_{L_1}	371 mΩ	282 mΩ
r_{L_2}	118 mΩ	108 mΩ	r_{L_2}	373 mΩ	292 mΩ
			f_p	200 kHz	200 kHz
			C_p	-	100 μF

Namely, we obtain

$$Ds_{plb} \leq Ds_{pmin} = Ds_{pr}, \tag{45}$$

and

$$Ds_{pmax} = \frac{k_r Ds_{pr}}{k_{min}} \leq Ds_{pub}, \tag{46}$$

where Ds_{pr} and k_r are the duty ratio of the regulator and coupling coefficient in the rated condition. Note that (46) considers the fact that the product of the coupling coefficient and duty ratio is kept constant during the regulation, as given in (32).

The system is optimized for achieving maximum efficiency in the rated condition. Besides, the duty ratio of the buck converter should be in the specified range. Therefore, the optimization problem is formulated using (45) and (46) as

$$\max_{\boldsymbol{x}} F(\boldsymbol{x}) = \eta(\boldsymbol{x}),$$

$$\text{subject to} \quad Ds_{plb} \leq Ds_{pr} \leq \frac{k_{min} Ds_{pub}}{k_r},$$

Tables 3 and 4 give the optimized parameter set and component values provided by the PSO algorithm, respectively.

B. IMPLEMENTED PROTOTYPE

Table 4 also gives the component values on the implemented circuit, measured by the Keysight E4990A impedance analyzer. The measured shunt capacitance C_S does not include the parasitic capacitance of the switching device in Table 4. In the obtained optimal coil parameters, the coupling coefficient between L_1 and L_2 varied within $0.072 \leq k \leq 0.15$ in the range of $1 \leq d_c/d_{cr} \leq 2$. Table 5 gives the selected devices in the experiment. Fig. 9 shows the implemented LI class-E/F WPT system with post regulator.

TABLE 5. Circuit devices in the implemented system.

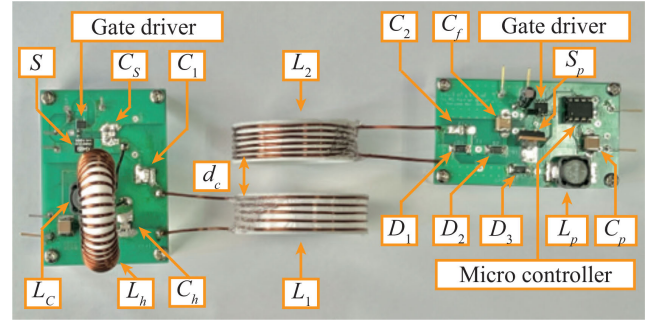| Component	Device	Manufacturer	Key parameters
S	GS66502B	GaN Systems	$\alpha_o = 1.6, \beta_o = 1.6,$ $k_o = 3.5 \times 10^{-16}$ $r_{on} = 0.26\ \Omega$
S_p	IRF530	Vishay	$r_{onp} = 0.16\ \Omega, C_{op} = 250$ pF
$D_i\ (i = 1, 2, 3)$	STPS5H100AF	STMicroelectronics	
Gate driver for S	UCC27512	Texas Instruments	
Gate driver for S_p	IR2011	Infineon	
L_C	MSS1278H-124	Coilcraft	$L_C = 120\ \mu$H
L_p	MSS1278H-224	Coilcraft	$L_p = 220\ \mu$H

FIGURE 9. Photo of the implemented LI class-E/F WPT system with post regulator.

C. PERFORMANCE EVALUATION

Fig. 10 shows the analytical and experimental waveforms of the LI WPT system without the post regulator. We see from Fig. 10 that the switch voltages satisfied ZVS conditions even when R_L and k varied from the rated condition. The output voltage v_O for the same d_c was almost the same level because v_O is constant against load variations in the LI operation, as shown in (32). However, it is seen from Fig. 10(a)-(c) and (d)-(f) that the output voltage varied against coil misalignment due to the variation of k.

Fig. 11 shows the analytical and experimental waveforms of the system with the post regulator. We can see from Fig. 11 that the output voltage was regulated for all the coil distances, which was not achieved in Fig. 10. Moreover, all the switch voltages achieved the ZVS. This is because the equivalent inductance seen from the inverter kept constant against not only load variations but also coil misalignment. Therefore, we confirmed that the post-regulator operation did not affect the soft switching condition of the inverter, namely maintaining the LI operation even for any coil distance in the proposed system. Notably, the proposed system does not require wireless communication from the receiver to the transmitter. The proposed WPT system achieves ZVS and output regulation against both load variations and coil misalignment. The experiments demonstrated the effectiveness of the proposed system.

Fig. 12 shows the analytical and experimental output voltage V_O and the duty ratio of the post regulator Ds_p as functions of the normalized load resistance and coil distance, respectively. The output voltage of the LI WPT system without the post regulator increases gradually as the load resistance increases, as shown in Fig. 12(a). This is due to the parasitic capacitance of the diodes. Although the induced
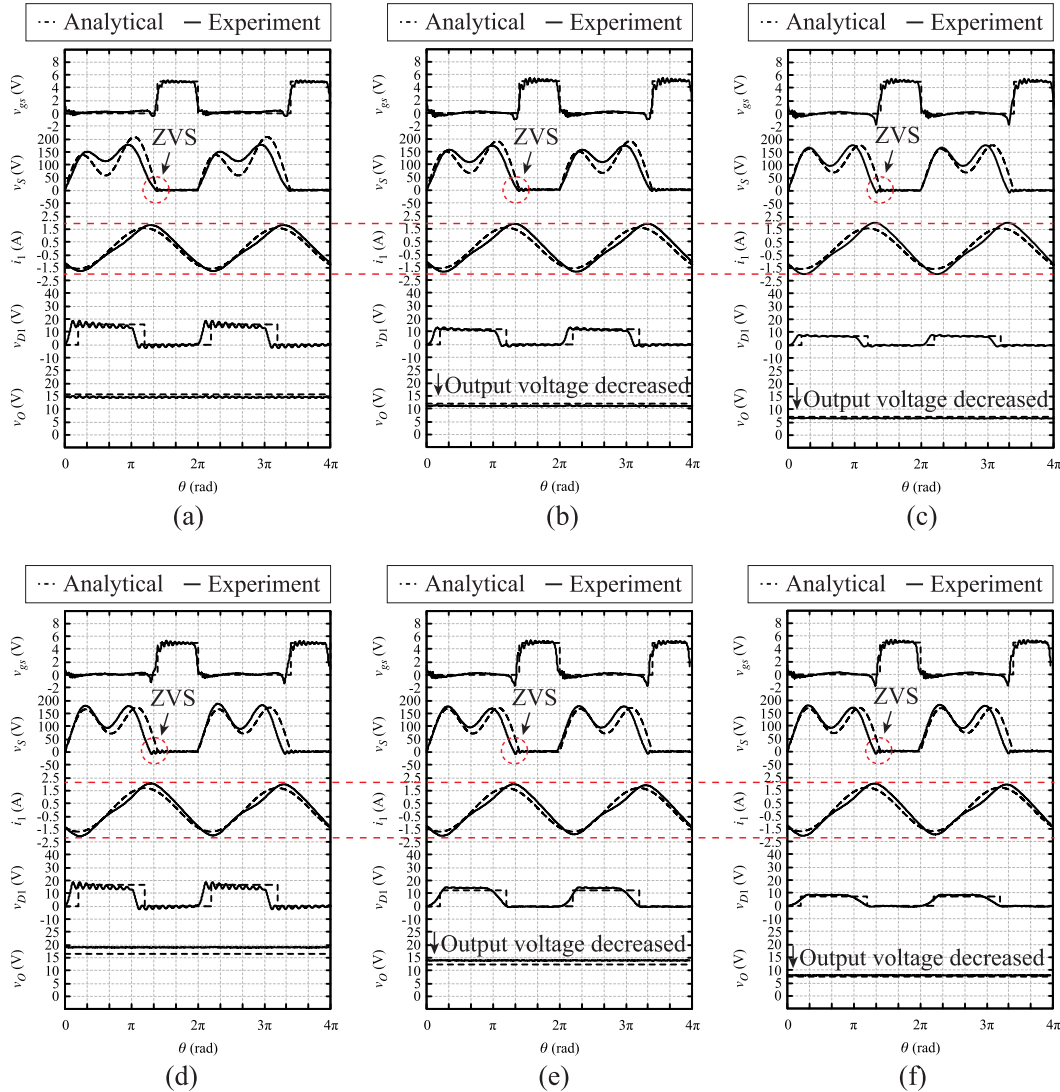
FIGURE 10. Analytical and experimental waveforms of the WPT system without post regulator. (a) For $R_L/R_{Lr} = 1$ and $d_c = 15$ mm. (b) For $R_L/R_{Lr} = 1$ and $d_c = 20$ mm. (c) For $R_L/R_{Lr} = 1$ and $d_c = 30$ mm. (d) For $R_L/R_{Lr} = 10$ and $d_c = 15$ mm. (e) For $R_L/R_{Lr} = 10$ and $d_c = 20$ mm. (f) For $R_L/R_{Lr} = 10$ and $d_c = 30$ mm.

voltage of the receiver is constant regardless of the load resistance, the rise and fall times of v_{D1} increase, as shown in Fig. 10(d)-(f), compared with Fig. 10(a)-(c). Therefore, the maximum value of v_{D1} increases, which causes the output voltage to increase. On the other hand, the system with the post regulator keeps a constant output voltage by slightly changing the duty ratio of the regulator.

We can see from Fig. 12(b) that the output voltage is kept constant in the system with the post regulator, though it significantly decreased in the system without the post regulator. Therefore, the duty ratio of the post regulator increased as the coil distance became longer in the system with the post regulator. We can confirm that the post regulator works mainly against the coil misalignment, which did not interfere with LI operating conditions.

Fig. 13 shows the analytical and experimental power delivery efficiency η as a function of the normalized load

resistance and coil distance, respectively. We can see from Fig. 13(a) that the efficiency of the system with the post regulator is slightly less than that without the post regulator due to the additional regulator. On the other hand, the efficiency of the system with post regulator is kept high against coil misalignment, as shown in Fig. 13(b). This is because the equivalent resistance seen from the inverter is kept constant against the coil misalignment due to the impedance transformation, as given in (23). Therefore, the power losses in the transmitter are almost constant against coil misalignment in the system with the post regulator.

Fig. 14 shows the analytical power-loss breakdown, which is calculated based on the analysis in Section IV-E. The experimental total power loss is also plotted in Fig. 14. The subscript of 'P' in the box of Fig. 14 represents the power-loss factor. We can see from Fig. 14(a) that the power losses on the transmitter side, especially P_S, P_{L_h}, and P_{L_1}, are almost
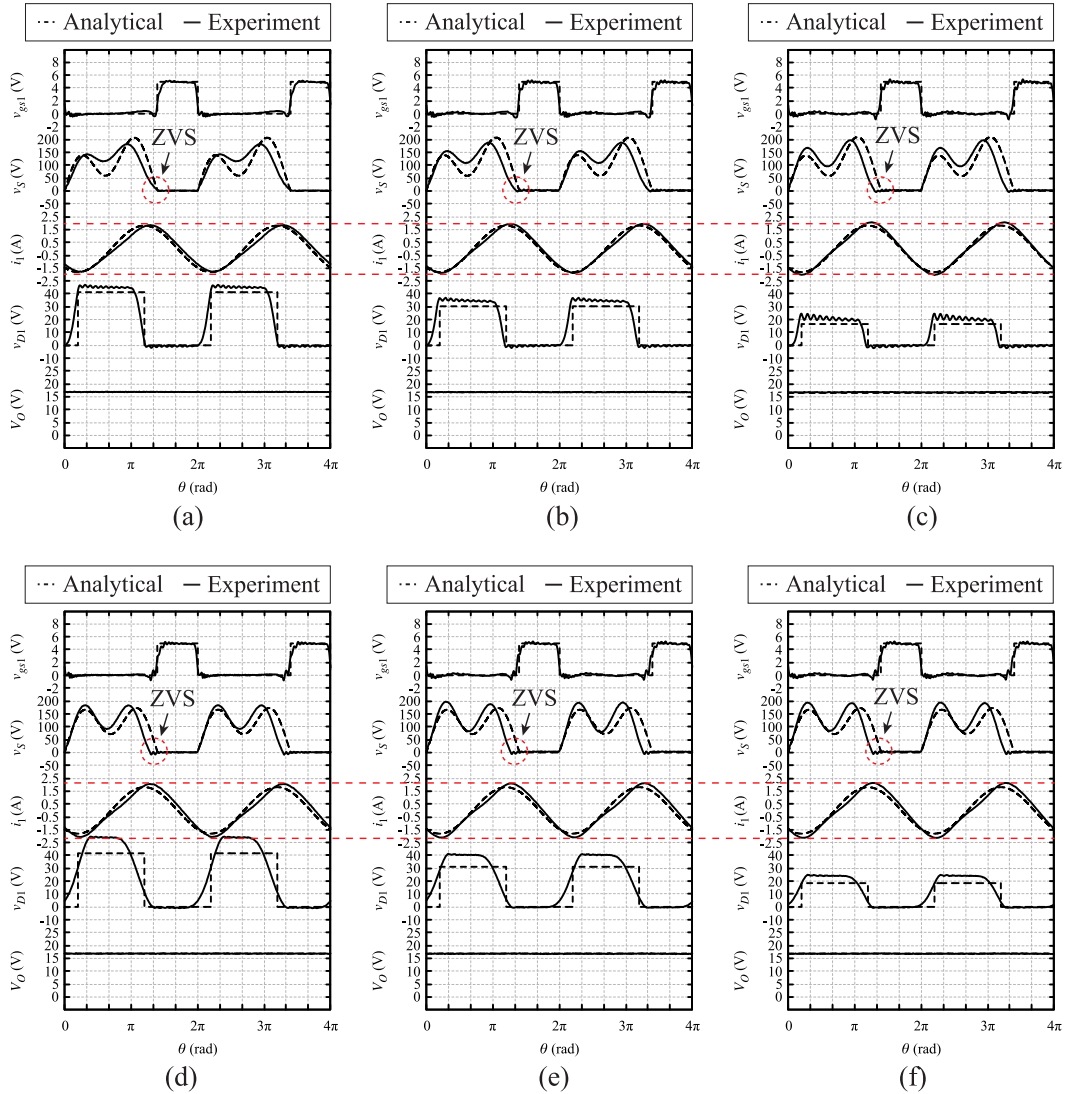
FIGURE 11. Analytical and experimental waveforms of the WPT system with post regulator. (a) For $R_L/R_{Lr} = 1$ and $d_c = 15\ mm$. (b) For $R_L/R_{Lr} = 1$ and $d_c = 20\ mm$. (c) For $R_L/R_{Lr} = 1$ and $d_c = 30\ mm$. (d) For $R_L/R_{Lr} = 10$ and $d_c = 15\ mm$. (e) For $R_L/R_{Lr} = 10$ and $d_c = 20\ mm$. (f) For $R_L/R_{Lr} = 10$ and $d_c = 30\ mm$.

constant over the entire load range. This is because the LI class-E/F inverter exhibits CC operation, and the conduction losses in each component become almost constant against load variations. On the other hand, the power losses on the receiver side decrease as the increase in load resistance because the current flowing through the receiver decreases at light load. It is seen from Fig. 14(b) that the power losses on the transmitter side are consistent against coil distance. This is because the impedance seen from the transmitter side is constant in the condition of $kDs_p = k_rDs_{pr}$ as given in (23). The receiver power loss increases for longer coil distances due to the increased receiver current. Because the power loss increase is much lower than the rated output power, the power delivery efficiency decreases slightly against coil misalignment, as shown in Fig. 13(b).

From the analytical and experimental results, we can confirm that the WPT system with the post regulator

is robust against load variations and coil misalignments without wireless communication feedback from transmitter to receiver. Besides, we confirmed that the output voltage regulation does not degrade the LI operation of the inverter from a comparison between the system with and without the regulator. All the errors between the analysis and experiment could be explained. The agreements between analytical and experimental results showed the accuracy of the analytical expressions.

VI. COMPARISON WITH PREVIOUS WORKS
There have been WPT systems that are robust against load variations and coil misalignment. Table 6 gives a comparison with previous works. In [37], a post regulator is used to maximize the efficiency against load variations and coil misalignment. In addition, [38] adds an impedance-matching network to achieve maximum efficiency and output-voltage

TABLE 6. Comparison with previous works.

|	[37]	[38]	[9]	[10]	[24]	This work
Transmission frequency	13.56 MHz	100 kHz	6.78 MHz	6.78 MHz	3.39 MHz	6.78 MHz
Inverter	Class-D	Class-D	Class-E	Class-E	LI class-E	LI class-E/F
Rectifier	Class-D	Class-D	Class-D	Class-E	Class-D	Class-D
Additional circuit	Post regulator	Impedance matching	Post regulator	Impedance matching	No	post regulator
Wireless communication	Yes	Yes	Yes	Yes	No	No
Output regulation for load variation	Yes	Yes	Yes	Yes	Yes	Yes
Soft switching for load variation	No	No	Yes	Yes	Yes	Yes
Output regulation for coil misalignment	Yes	Yes	Yes	Yes	No	Yes
Soft switching for coil misalignment	No	No	Yes	Yes	No	Yes
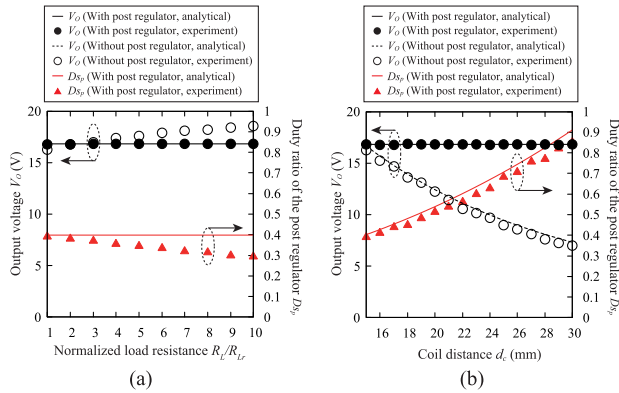
FIGURE 12. Analytical and experimental output voltage V_O and duty ratio of the post regulator Ds_P. (a) As a function of the normalized load resistance at $d_c = 15mm$. (b) As a function of the coil distance d_c at $R_L/R_{Lr} = 1$.
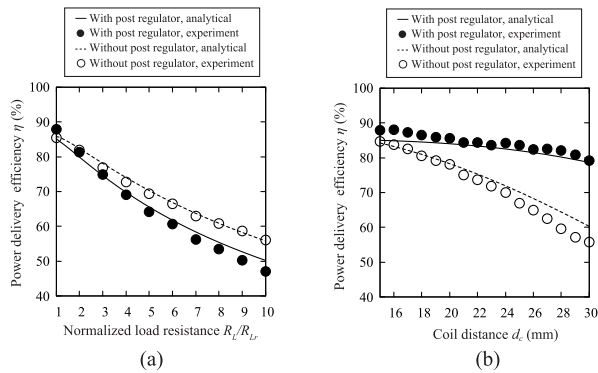

FIGURE 13. Analytical and experimental power delivery efficiency η. (a) As a function of the normalized load resistance at $d_c = 15mm$. (b) As a function of the coil distance d_c at $R_L/R_{Lr} = 1$.

regulation simultaneously. However, these works have been considered on the class-D inverter, which does not achieve soft switching. Also, these systems require wireless communication between the transmitter and receiver. In [9] and [10], maximum efficiency tracking control is proposed for the class-E WPT systems. Although these systems achieve soft switching over a wide range of load variations and coil misalignments, they require feedback communication. A comprehensive design procedure for a WPT system with the LI class-E inverters is presented in [24]. Soft switching and constant output are achieved against load variations without wireless communication by using LI inverters.
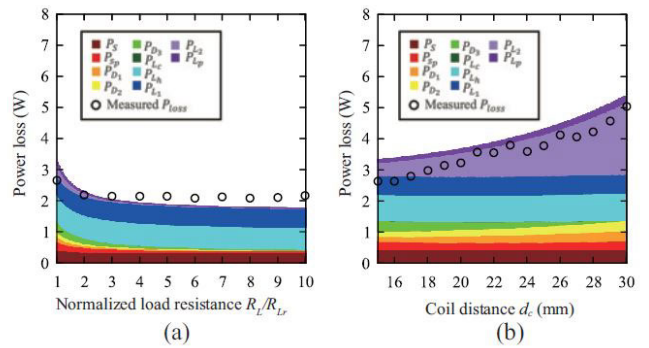

FIGURE 14. Analytical power-loss breakdown and measured P_{loss} of the system. (a) As a function of normalized load resistance at $d_c = 15mm$. (b) As a function of coil distance at $R_L/R_{Lr} = 1$.

However, this research addresses only load variations at fixed coil positions.

The design condition for achieving the LI operation of the inverter and output regulation is updated from Table 2 by considering the coil misalignments. Against load variation solely, the LI operation of the inverter and output regulation is achieved for all the coupling types. Meanwhile, it is limited only to S-S coupling having a specific rectifier when the coil misalignment is also considered. The obtained design guideline suggests that the transmitter topology is limited to the series-resonant LI inverters, for example, in [12], [13], [14], and [17], as given in Table 1. Based on the obtained design guideline, we can state that there is a case where the LI operation cannot be achieved by simply applying the post regulator. For example, the LI operation cannot be achieved against coil misalignment if the post regulator is added to the LI WPT system proposed in [24].

Also, there are some papers that discuss the stability and control methods of post regulators [39], [40]. It is known that the difference between the transmission frequency and the post-regulator frequency causes oscillation [40]. In the proposed system, the transmission frequency is sufficiently high compared to the post-regulator frequency. Therefore, the oscillation frequency component can be absorbed by the output capacitor of the rectifier. Namely, the post regulator can be controlled stably in the proposed system.

VII. CONCLUSION
This paper has presented an analysis and design of the LI high-frequency WPT system with robustness against load

variations and coil misalignments. The analysis has revealed that robustness against load variations and coil misalignment is obtained only when LI inverter, S-S coupling, input-reactance invariant rectifier against load variations, and post regulator are adopted. Under the derived system configuration, the WPT system achieves soft switching and output-voltage regulation without wireless communication between the receiver and transmitter. Based on the analysis, the design example of the system with LI class-E/F inverter, class-D rectifier, and buck converter was given. The quantitative agreements between the analytical prediction and experiment show the effectiveness and validity of the system and its analysis. We achieved 87.8 % power delivery efficiency with 6.78 *MHz* transmission frequency at the rated condition.

REFERENCES

[1] Y. Shao, H. Zhang, M. Liu, and C. Ma, "Explicit design of impedance matching networks for robust MHz WPT systems with different features," *IEEE Trans. Power Electron.*, vol. 37, no. 9, pp. 11382–11393, Sep. 2022.

[2] X. Meng, D. Qiu, M. Lin, S. C. Tang, and B. Zhang, "Output voltage identification based on transmitting side information for implantable wireless power transfer system," *IEEE Access*, vol. 7, pp. 2938–2946, 2019.

[3] M. Wagih, A. Komolafe, and B. Zaghari, "Dual-receiver wearable 6.78 MHz resonant inductive wireless power transfer glove using embroidered textile coils," *IEEE Access*, vol. 8, pp. 24630–24642, 2020.

[4] Y. Li, S. Liu, X. Zhu, J. Hu, M. Zhang, R. Mai, and Z. He, "Extension of ZVS region of series–series WPT systems by an auxiliary variable inductor for improving efficiency," *IEEE Trans. Power Electron.*, vol. 36, no. 7, pp. 7513–7525, Jul. 2021.

[5] J. Zhang, J. Zhao, L. Mao, J. Zhao, Z. Jiang, and K. Qu, "ZVS operation of class-E inverter based on secondary side zero compensation switching at variable coupling coefficient in WPT," *IEEE Trans. Ind. Appl.*, vol. 58, no. 1, pp. 1022–1031, Jan. 2022.

[6] H. Zhang, Y. Shao, M. Liu, and C. Ma, "A wide-load-range and compact MHz wireless power transfer system based on novel reactance compression design and edge inductor," *IEEE Trans. Power Electron.*, vol. 36, no. 10, pp. 11183–11195, Oct. 2021.

[7] S. Ghadeer, N. Rezaei-Hosseinabadi, A. Tabesh, and S. A. Khajehoddin, "Improving wireless power transfer efficiency considering rectifier input impedance and load quality factor," *IEEE Access*, vol. 11, pp. 61738–61747, 2023.

[8] S. Pahlavan, M. Shooshtari, and S. J. Ashtiani, "Star-shaped coils in the transmitter array for receiver rotation tolerance in free-moving wireless power transfer applications," *Energies*, vol. 15, no. 22, p. 8643, Nov. 2022.

[9] Y. Liu and H. Feng, "Maximum efficiency tracking control method for WPT system based on dynamic coupling coefficient identification and impedance matching network," *IEEE J. Emerg. Sel. Topics Power Electron.*, vol. 8, no. 4, pp. 3633–3643, Dec. 2020.

[10] Y. Shao, N. Kang, H. Zhang, R. Ma, M. Liu, and C. Ma, "A lightweight and robust drone MHz WPT system via novel coil design and impedance matching," *IEEE Trans. Ind. Appl.*, vol. 59, no. 3, pp. 3851–3864, May/Jun. 2023.

[11] Y. Li, J. Hu, M. Liu, Y. Chen, K. W. Chan, Z. He, and R. Mai, "Recon-figurable intermediate resonant circuit based WPT system with load-independent constant output current and voltage for charging battery," *IEEE Trans. Power Electron.*, vol. 34, no. 3, pp. 1988–1992, Mar. 2019.

[12] R. E. Zulinski and K. J. Grady, "Load-independent class E power inverters. I. Theoretical development," *IEEE Trans. Circuits Syst.*, vol. 37, no. 8, pp. 1010–1018, Aug. 1990.

[13] L. Roslaniec, A. S. Jurkov, A. A. Bastami, and D. J. Perreault, "Design of single-switch inverters for variable resistance/load modulation operation," *IEEE Trans. Power Electron.*, vol. 30, no. 6, pp. 3200–3214, Jun. 2015.

[14] S. Aldhaher, P. D. Mitcheson, and D. C. Yates, "Load-independent class EF inverters for inductive wireless power transfer," in *Proc. IEEE Wireless Power Transf. Conf. (WPTC)*, May 2016, pp. 1–4.

[15] A. Komanaka, W. Zhu, X. Wei, K. Nguyen, and H. Sekiya, "Generalized analysis of load-independent ZCS parallel-resonant inverter," *IEEE Trans. Ind. Electron.*, vol. 69, no. 1, pp. 347–356, Jan. 2022.

[16] A. Komanaka, W. Zhu, X. Wei, K. Nguyen, and H. Sekiya, "Load-independent inverse class-E ZVS inverter and its application to wireless power transfer systems," *IET Power Electron.*, vol. 15, no. 7, pp. 644–658, May 2022.

[17] Y. Komiyama, W. Zhu, K. Nguyen, and H. Sekiya, "Load-independent constant-current/zero-current switching inverter with series resonant filter," in *Proc. IEEE Appl. Power Electron. Conf. Expo. (APEC)*, Mar. 2023, pp. 490–494.

[18] T. Sensui and H. Koizumi, "Load-independent class E zero-voltage-switching parallel resonant inverter," *IEEE Trans. Power Electron.*, vol. 36, no. 11, pp. 12805–12818, Nov. 2021.

[19] T. Sowlati, C. A. T. Salama, J. Sitch, G. Rabjohn, and D. Smith, "Low voltage, high efficiency GaAs class E power amplifiers for wireless transmitters," *IEEE J. Solid-State Circuits*, vol. 30, no. 10, pp. 1074–1080, Oct. 1995.

[20] R. Redl, B. Molnar, and N. O. Sokal, "Class e resonant regulated DC/DC power converters: Analysis of operations, and experimental results at 1.5 MHz," *IEEE Trans. Power Electron.*, vol. PE-1, no. 2, pp. 111–120, Apr. 1986.

[21] A. Kurs, A. Karalis, R. Moffatt, J. D. Joannopoulos, P. Fisher, and M. Soljačić, "Wireless power transfer via strongly coupled magnetic resonances," *Science*, vol. 317, no. 5834, pp. 83–86, Jul. 2007.

[22] S. Aldhaher, D. C. Yates, and P. D. Mitcheson, "Load-independent class E/EF inverters and rectifiers for MHz-switching applications," *IEEE Trans. Power Electron.*, vol. 33, no. 10, pp. 8270–8287, Oct. 2018.

[23] W. Zhu, Y. Komiyama, K. Nguyen, and H. Sekiya, "Comprehensive and simplified numerical design procedure for class-E switching circuits," *IEEE Access*, vol. 9, pp. 149971–149981, 2021.

[24] H. Sekiya, K. Tokano, W. Zhu, Y. Komiyama, and K. Nguyen, "Design procedure of load-independent class-E WPT systems and its application in robot arm," *IEEE Trans. Ind. Electron.*, vol. 70, no. 10, pp. 10014–10023, Oct. 2023.

[25] W. Luo, Y. Ogi, F. Ebihara, X. Wei, and H. Sekiya, "Design of load-independent class-E inverter with MOSFET gate-to-drain and drain-to-source parasitic capacitances," *Nonlinear Theory Appl.*, vol. 11, no. 2, pp. 267–277, 2020.

[26] Y. Wang, W. Liu, and Y. Huangfu, "Design of wireless power transfer system with load-independent voltage/current output based on the double-sided CLC compensation network," in *Proc. IEEE Transp. Electrific. Conf. Expo (ITEC)*, Jun. 2019, pp. 1–5.

[27] K. Voottipruex, E. Mujjalinvimut, A. Sangswang, and S. Naetiladdanon, "A load-independent operation of WPT under frequency bifurcation for battery charging applications," in *Proc. 46th Annu. Conf. IEEE Ind. Electron. Soc. (IECON)*, Oct. 2020, pp. 2573–2578.

[28] Y. Komiyama, S. Matsuhashi, W. Zhu, T. Mishima, Y. Ito, T. Uematsu, K. Nguyen, and H. Sekiya, "Frequency-modulation controlled load-independent class-E inverter," *IEEE Access*, vol. 9, pp. 144600–144613, 2021.

[29] M. K. Kazimierczuk and D. Czarkowski, *Resonant Power Converters*. Hoboken, NJ, USA: Wiley, 2011.

[30] J. Ma, Asiya, X. Wei, K. Nguyen, and H. Sekiya, "Analysis and design of generalized class-E/F2 and class-E/F3 inverters," *IEEE Access*, vol. 8, pp. 61277–61288, 2020.

[31] M. K. Kazimierczuk, *Pulse-Width Modulated DC–DC Power Converters*. Hoboken, NJ, USA: Wiley, 2008.

[32] G. Zulauf, S. Park, W. Liang, K. N. Surakitbovorn, and J. Rivas-Davila, "COSS losses in 600 V GaN power semiconductors in soft-switched, high-and very-high-frequency power converters," *IEEE Trans. Power Electron.*, vol. 33, no. 12, pp. 10748–10763, Dec. 2018.

[33] H. Nagaoka, "The inductance coefficients of solenoids," *J. College Sci.*, vol. 27, no. 6, pp. 1–33, 1909.

[34] P. J. Dowell, "Effects of eddy currents in transformer winding," *Proc. IEE*, vol. 113, no. 8, pp. 1387–1394, Aug. 1966.

[35] M. K. Kazimierczuk, *High-Frequency Magnetic Components*. Hoboken, NJ, USA: Wiley, 2014.

[36] J. Kennedy and R. Eberhart, "Particle swarm optimization," in *Proc. Int. Conf. Neural Netw.*, vol. 4, Nov./Dec. 1995, pp. 1942–1948.

[37] M. Fu, H. Yin, X. Zhu, and C. Ma, "Analysis and tracking of optimal load in wireless power transfer systems," *IEEE Trans. Power Electron.*, vol. 30, no. 7, pp. 3952–3963, Jul. 2015.

[38] M. Fu, H. Yin, M. Liu, and C. Ma, "Loading and power control for a high-efficiency class E PA-driven megahertz WPT system," *IEEE Trans. Ind. Electron.*, vol. 63, no. 11, pp. 6867–6876, Nov. 2016.

[39] K. Li, H. Yuan, S.-C. Tan, and S. Y. R. Hui, "Overshoot damping and dynamics improvement in wireless power transfer systems via receiver-side controller design," *IEEE Trans. Power Electron.*, vol. 37, no. 2, pp. 2362–2371, 2022.

[40] K. Li, S.-C. Tan, and R. S. Y. Hui, "On beat frequency oscillation of two-stage wireless power receivers," *IEEE Trans. Power Electron.*, vol. 35, no. 12, pp. 12741–12751, Dec. 2020.

YUTARO KOMIYAMA (Graduate Student Member, IEEE) was born in Nagano, Japan, in June 1998. He received the B.E. and M.E. degrees from Chiba University, Japan, in 2021 and 2022, respectively, where he is currently pursuing the Ph.D. degree with the Graduate School of Science and Engineering. His research interests include high-frequency inverters and power oscillators and their applications for wireless power transfer systems.

AYANO KOMANAKA was born in Aichi, Japan, in August 1997. She received the B.E. and M.E. degrees from Chiba University, Japan, in 2020 and 2022, respectively, where she is currently pursuing the Ph.D. degree with the Graduate School of Science and Engineering. Her research interests include about high-frequency and high-efficiency inverters.

HIROAKI OTA received the B.E. degree in electrical, electronic, and information engineering from the National Institute of Technology, Nara College (NITNC), Nara, Japan, in 2018, and the M.E. degree in electrical, electronic, and information engineering from Osaka University, Osaka, Japan, in 2020. Since 2020, he has been with Omron Corporation, Kyoto, Japan. His research interest includes wireless power transfer systems.

YUKI ITO received the B.S. and M.S. degrees from the Interdisciplinary Faculty of Science and Engineering, Shimane University. He is currently with OMRON Corporation Ltd., Kyoto, Japan. He has been engaged in the development of various power supplies, especially the F.A. power supply.

TAICHI MISHIMA received the B.S. and M.S. degrees from the Interdisciplinary Faculty of Science and Engineering, Shimane University. He is currently with Omron Corporation Ltd., Kyoto, Japan. He has been engaged in the development of various DC/DC converters.

TAKESHI UEMATSU received the B.E. degree in precision mechanical engineering from Tokyo Denki University, Japan, in 1986, the M.S. degree in electronics and computer science from Tsukuba University, Japan, in 1992, and the Ph.D. degree in information science and electrical engineering from Kyusyu University, Japan, in 2011. In 2017, he joined Omron Corporation Ltd. He has over 30 years of experience developing AC/DC and DC/DC converters.

AKIHIRO KONISHI (Member, IEEE) received the B.S. degree in electrical engineering from the Faculty of Advanced Engineering, National Institute of Technology, Nara College (NITNC), Nara, Japan, in 2017, and the M.S. and Ph.D. degrees in electrical engineering from Okayama University, Okayama, Japan, in 2019 and 2023, respectively. He is currently a Project Assistant Professor with Chiba University, Chiba, Japan. His research interests include a wireless power transfer systems and the design of a controller for a high-frequency switching circuit.

WENQI ZHU (Member, IEEE) was born in Hefei, Anhui, China. He received the B.E. degree from Anhui University, China, in 2016, and the M.E. and Ph.D. degrees from Chiba University, Japan, in 2020 and 2022, respectively. He is currently a Postdoctoral Fellow with Chiba University. His current research interests include DC/DC, AC/DC power converters, and WPT systems.

KIEN NGUYEN (Senior Member, IEEE) received the B.E. degree in electronics and telecommunication from the Hanoi University of Science and Technology (HUST), Vietnam, in 2004, and the Ph.D. degree in informatics from the Graduate University for Advanced Studies, Japan, in 2012. He was a Researcher with the National Institute of Information and Communication Technology (NICT), Japan, from 2014 to 2018. Since 2018, he has been with the Graduate School of Engineering, Chiba University, where he is currently an Associate Professor. His research interests include a wide range of topics in networking and distributed systems, including the Internet, the Internet of Things technologies, and distributed ledger technologies.

HIROO SEKIYA (Senior Member, IEEE) was born in Tokyo, Japan, in July 1973. He received the B.E., M.E., and Ph.D. degrees in electrical engineering from Keio University, Yokohama, Japan, in 1996, 1998, and 2001, respectively. Since April 2001, he has been with Chiba University, Chiba, Japan, where he is currently a Professor with the Graduate School of Engineering. From February 2008 to February 2010, he was with the Department of Electrical Engineering, Wright State University, Dayton, OH, USA, as a Visiting Scholar. His research interests include high-frequency inverters, resonant converters, wireless power transfer systems, wireless communication system designs, and nonlinear circuit theory.

● ● ●